

1 Neutron-Neutron Correlations in the Photofission of U-238

2 J. Burggraf, D.S. Dale, and T. Forest
3

4 *Department of Physics,
5 Idaho State University, Pocatello, ID 83201*

6 G. Warren, S. Stave, S. Behling, and E. Church
7

8 *Pacific Northwest National Laboratory, PO Box 999, Richland, Washington 99352*

(Dated: March 12, 2019)

9 **Background:** In the fission of actinides, the nearly back-to-back motion of the fission fragments has a strong
10 effect on the kinematics of fission neutrons. This leads to a favoring of opening angles near 0° and 180° in the
11 neutron-neutron (n-n) opening angle distributions of correlated neutron pairs from the same fission event.

12 **Purpose:** To measure the n-n opening angle and energy correlations in the photofission of ^{238}U . As of this
13 writing, measurements of correlated n-n opening angle distributions have been reported only for the spontaneous
14 and neutron-induced fission of actinides. This work is the first to report such a measurement using photofission
15 and will provide useful experimental input for photofission models used in codes such as MCNP and FREYA.

16 **Method:** Fission is induced using bremsstrahlung photons produced via a low duty factor, pulsed, linear electron
17 accelerator. The bremsstrahlung photon beam impinges upon a ^{238}U target that is surrounded by a large neutron
18 scintillation detection system capable of measuring particle position and time of flight, from which n-n opening
19 angle and energy are measured. Neutron-neutron angular correlations are determined by taking the ratio between
20 a correlated neutron distribution and an uncorrelated neutron distribution formed by the pairing of neutrons pro-
21 duced during different beam pulses. This analysis technique greatly diminishes effects due to detector efficiencies,
22 acceptance, and experimental drifts.

23 **Results:** The angular correlation of neutrons from the photofission of ^{238}U shows a high dependence on neutron
24 energy as well as a dependence on the angle of the emitted neutrons with respect to the incoming photon beam.
25 Angular correlations were also measured using neutrons from the spontaneous fission of ^{252}Cf , showing good
26 agreement with past measurements.

27 **Conclusions:** The measured angular correlations reflect the underlying back-to-back nature of the fission frag-
28 ments. An anomalous decline in n-n yield was observed for opening angles near 180° .

29 CONTENTS

30 I. Overview of Neutron-Neutron Angular
31 Correlations in Fission
32 A. Theoretical Basis
33 B. Past Measurements: Spontaneous and
34 Neutron Induced Fission
35 C. Considerations for Photofission

36 II. Experimental Setup
37 A. Detectors
38 B. Detector Shielding
39 C. Bremsstrahlung Photon Beam
40 D. DU Target
41 E. Electronics

42 III. Measurement Techniques
43 A. Particle Time of Flight and Energy
44 Determination
45 B. Particle Position Reconstruction
46 C. Measurements with ^{252}Cf

47 IV. Analysis
48 A. Cancelation of Detector Efficiencies, Drifts,
49 and Geometric Phase Space
50 B. Subtraction of Accidental Coincidences

51 V. Potential sources of error

52 A. Correlated versus uncorrelated n-n energy
53 distribution
54 B. Detector Cross-talk
55 1. Simulation of Detector Cross-talk
56 C. Neutron Scattering within the Target

57 VI. Results

58 A. n-n angular correlation versus neutron
59 energy
60 B. Considering θ_{abs}

61 VII. Concluding Remarks

62 VIII. Acknowledgments

63 References

64 I. OVERVIEW OF NEUTRON-NEUTRON 65 ANGULAR CORRELATIONS IN FISSION

66 The fission process is characterized by the emission of
67 neutrons. Neutron emission in fission can be classified
68 into two categories depending on the time of emission:
69 delayed and prompt. Prompt fission neutrons are de-
70 fined as neutrons that are emitted either immediately

71 after ($< 10^{-14}$ seconds) fission, or, during the scission
 72 of the nucleus, and account for $\sim 99\%$ of neutron emis-
 73 sion [2]. Delayed neutrons are not relevant to the present
 74 work because they account for only $\sim 1\%$ of total neu-
 75 tron emission in actinide photofission [2], and, they are
 76 emitted milliseconds to minutes after fission, which is
 77 well outside the neutron acceptance timing window of
 78 the present work.

79 Prompt fission neutron production occurs by means of
 80 two distinct mechanisms. The dominant mechanism is
 81 neutron emission from the fully accelerated fragments.
 82 The second mechanism, referred to as *early* or *scission*
 83 neutron emission, is the emission of neutrons during ei-
 84 ther the scission of the nucleus or the acceleration of the
 85 fission fragments. A large number of past studies have
 86 established that the majority of prompt fission neutrons
 87 (80%–98%) are emitted from the fully accelerated frag-
 88 ments, while scission neutrons account for the remaining
 89 2%–20% percent [3]. The nature of scission neutrons has
 90 remained elusive since their first tentative observation in
 91 1962 by Bowman *et al.* [4].

92 A. Theoretical Basis

93 The neutron-neutron (n-n) opening angle distribution
 94 of correlated neutron pairs, as seen in the lab frame, is
 95 widely used for the quantification of n-n angular corre-
 96 lations. Angular correlations in fission neutrons arise due
 97 to the kinematics of the fission fragments. It has been
 98 shown that neutrons released from the fully accelerated
 99 fission fragments are evaporated isotropically in the frag-
 100 ment’s rest frame, and are emitted at speeds compara-
 101 ble to that of the fragments themselves [5]. This leads
 102 to the well-known U-shaped distribution in neutron-
 103 neutron opening angle (θ_{nn}), which has been reported
 104 in studies of neutron-induced, spontaneous, and, in this
 105 work, photofission. An example of a typical θ_{nn} distri-
 106 bution is seen in Fig. 1.

107 The U-shaped distribution of θ_{nn} can be understood
 108 as the result of the boost provided to the neutrons by the
 109 fission fragments in binary fission. Due to the conserva-
 110 tion of momentum, the fully accelerated fission fragments
 111 are traveling nearly back-to-back, and neutrons emitted
 112 from different fragments are boosted in opposite direc-
 113 tions, whereas neutrons emitted from the same fragment
 114 are boosted in the same direction. Thus, because the
 115 velocities of the fission fragments are large enough to ac-
 116 count for a significant portion of the kinetic energy of fis-
 117 sion neutrons, neutron pairs emitted from the accelerated
 118 fragments exhibit a favoring of opening angles near 0° if
 119 emitted from the same fragment and 180° if emitted from
 120 different fragments, and, consequently, a suppression of
 121 opening angles near 90° .

122 The favoring of large and small n-n opening angles
 123 shows a strong dependence on neutron energy. Neutrons
 124 with higher energy are more likely to have been emitted
 125 along the same direction as the fission fragments and are

126 therefore expected to favor large and small opening an-
 127 gles. The θ_{nn} distribution and its dependence on neutron
 128 energy are expected to shed light on several fundamental
 129 aspects of the fission process including the neutron mul-
 130 tiplicity distributions associated with the light and heavy
 131 fission fragments, the nuclear temperatures of the fission
 132 fragments, and the mass distribution of the fission frag-
 133 ments as a function of energy released. In addition, the
 134 unique kinematics of fission and the resulting n-n corre-
 135 lations have the potential to be the basis for a new tool
 136 to characterize fissionable materials [6].

137 B. Past Measurements: Spontaneous and Neutron 138 Induced Fission

139 The first measurement of the angular correlation
 140 among coincident neutrons from fission was performed
 141 by Debenedetti *et al.* [7] in 1948 from neutron induced
 142 fission of ^{235}U . The next measurement of this type was
 143 performed by Pringle and Brooks in 1975 [8], in which
 144 neutrons emitted from the spontaneous fission (SF) of
 145 ^{252}Cf were found to have high coincidence rates at small
 146 opening angles near 0° and large opening angles near
 147 180° . In order to produce a result that is insensitive
 148 to the effects of detector geometry and efficiency, the
 149 present work uses techniques similar to those used in ref-
 150 erence [8], in which a ratio is taken between a correlated
 151 opening angle distribution and an uncorrelated opening
 152 angle distribution.

153 To date, numerous measurements of n-n angular cor-
 154 relation using ^{252}Cf have been performed [8–11]. This
 155 makes ^{252}Cf a good benchmark for n-n angular corre-
 156 lation measurements. Figure 1 compares measurements
 157 in this work to past measurements of n-n correlations in
 158 the SF of ^{252}Cf . Correlated n-n measurements have also
 159 been performed using thermal induced fission of ^{235}U ,
 160 ^{233}U , and ^{239}Pu [12].

162 C. Considerations for Photofission

163 The photofission reaction occurs during the de-
 164 excitation of a nucleus after the absorption of a pho-
 165 ton. For photon energies between 6 and 25 MeV, this ab-
 166 sorption occurs primarily via the giant dipole resonance
 167 (GDR). One distinct and useful aspect of photofission,
 168 relative to neutron-induced fission, is the low transfer of
 169 angular momentum to the nucleus, which gives rise to a
 170 simpler set of selection rules for the transfer of angular
 171 momentum. For the photofission of even-even nuclei, ex-
 172 citation occurs primarily via electric dipole transitions,
 173 and to a lesser extent electric quadrupole transitions,
 174 which gives rise to anisotropies in the fission fragment
 175 angular distribution that are far more pronounced than
 176 for other types of fission [1]. These anisotropies are ex-
 177 pressed in the angular distribution of emitted neutrons.
 178 For these reasons, photofission is increasingly being used

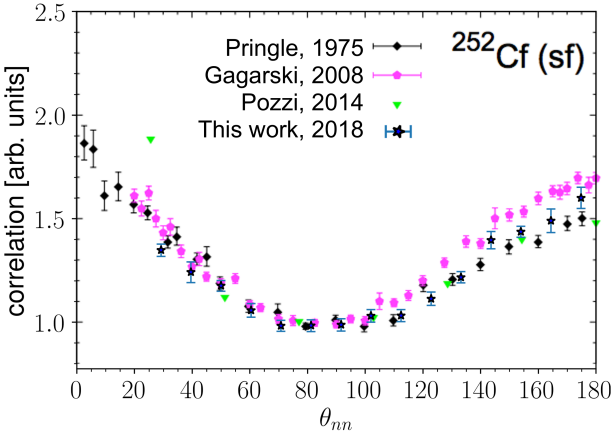


FIG. 1: θ_{nn} distribution from the spontaneous fission of ^{252}Cf . The neutron detection threshold for Pringle [8], Gagarski [11], and Pozzi [13] is 0.425 MeV, 0.425 MeV, and 0.7 MeV, respectively, and for this work is 0.5 MeV.

as a means to study sub-nuclear structures and the fundamentals of the fission process. Such studies are needed in order to dial in various model parameters required for an accurate theoretical description of the fission process.

II. EXPERIMENTAL SETUP

This experiment was carried out at the Idaho Accelerator Center (IAC), using their short-pulsed linear accelerator, which is an L-band frequency (1300 MHz) electron linear accelerator. See section II C for the accelerator parameters used during the experiment. Figure 2 shows a top-down diagram of the experimental arrangement.

The detection system measures neutron position and time of flight (ToF), which is defined as the time taken for a particle to travel from the fission target to a detector. The purpose of the ToF measurement is to determine the kinetic energy of detected neutrons and to distinguish between photons and neutrons. The detection system's positional precision is ± 9 cm, which gives an average angular precision of $\pm 6^\circ$ in opening angle reconstruction.

The detection system consists of fourteen shielded scintillators made from Polyvinyl Toluene (PVT) arranged in a ring around the target (see Figs. 2 and 3). Attached to both ends of each scintillator are 10-cm long, non-scintillating, ultra-violet transmitting, plastic light-guides. A Hamamatsu 580-17 photomultiplier (PMT) tube is fixed to each light-guide using optical glue. In order to increase the chance that scintillation light remains inside the scintillator, the scintillators were polished to remove micro-imperfections and were then wrapped in reflective aluminized mylar.

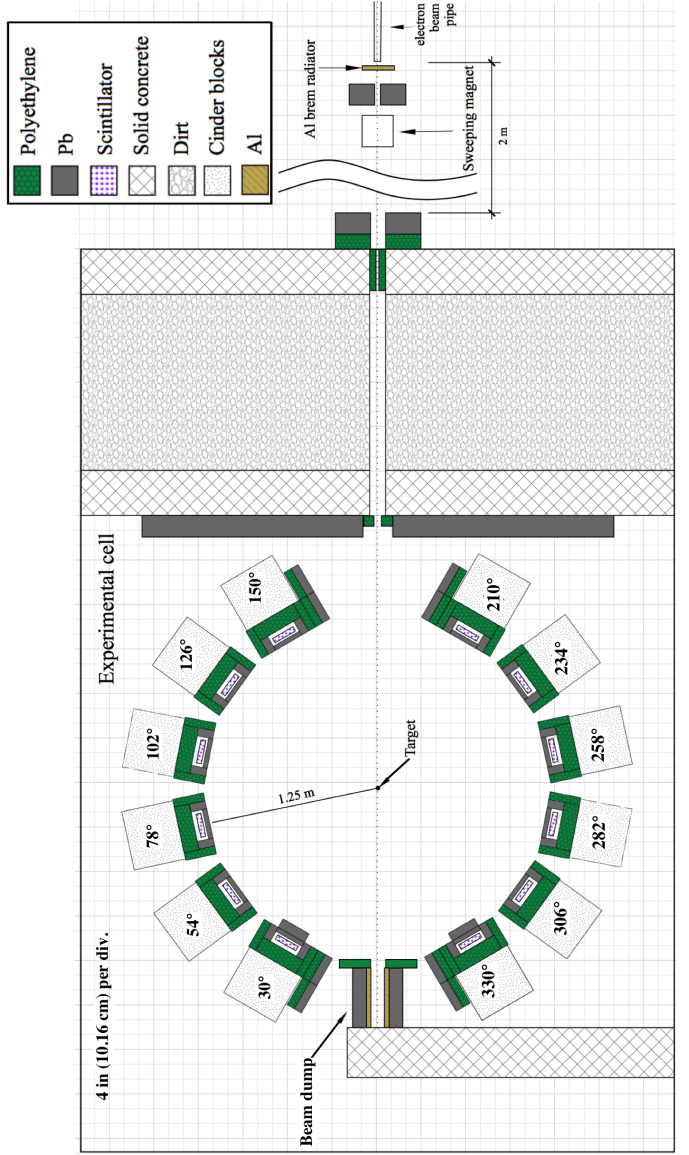


FIG. 2: To-scale, top down diagram of the experimental setup. An electron beam impinges upon a 3.8 cm thick Al radiator, and the resulting bremsstrahlung beam enters the experimental cell from the top. The supporting structure for each detector has been labeled according to the angle, in degrees, between the center of each detector and direction of the incoming photon beam.

Ten out of the fourteen scintillators had dimensions of $76.2 \times 15.2 \times 3.8$ cm 3 . The remaining four, the forward-most detectors located at $\pm 30^\circ$ with respect to the beam, had dimensions of $25.4 \times 15.2 \times 3.8$ cm 3 . These scintillators, 1/3 the length of the rest, are the result of the segmentation of two normally sized scintillators in order to address the high photon flux at these locations caused by the forward scattering of photons from the target. Prior to segmentation, a photon was registered in the forward-most detectors at a rate of about 0.9 photons per pulse, and because the electronics were operated in single hit

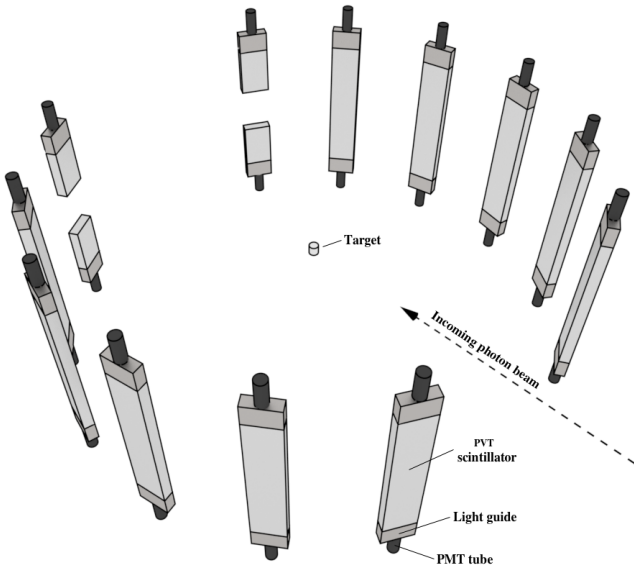


FIG. 3: 3-D render of the bare, unshielded scintillators, along with PMTs and light guides. Most of the open space between the scintillators was occupied by shielding, as seen in Fig. 2.

mode (see section II E), this greatly reduced the effective neutron detection efficiency. After segmentation and optimization of shielding, the photon detection rate was about 0.2 photons per pulse in each segmented detector. The segmented detectors also differ from the rest in that they were instrumented with only a single PMT, and therefore provide a comparatively lower precision in energy and position measurements. In order to test for systematic errors that may have resulted from the use of the segmented detectors, opening angle measurements were compared with and without their use, and the differences were well within experimental errors.

The relative efficiencies of the neutron detectors as a function of neutron energy were calculated by dividing measured and known yields from the SF of ^{252}Cf taken from MCNP. The results are shown in Fig. 4, which is produced from the aggregate of events in all detectors. See section IV for a discussion of how the effects of detector efficiency are accounted for in this work.

B. Detector Shielding

The detector shielding, depicted in Fig. 5, was constructed using lead and polyethylene with the aim of reducing detector cross-talk, the detection of photons, and noise. The sides of each scintillator were shielded with 5 cm of lead followed by 5 cm of polyethylene to reduce the chance of neutron cross-talk. Lead was not placed behind the scintillators after an MCNP-POLIMI simulation indicated that cross-talk would occur at significant rates otherwise. Instead, 10 cm of polyethylene was placed behind the scintillators. For a detailed discussion about the

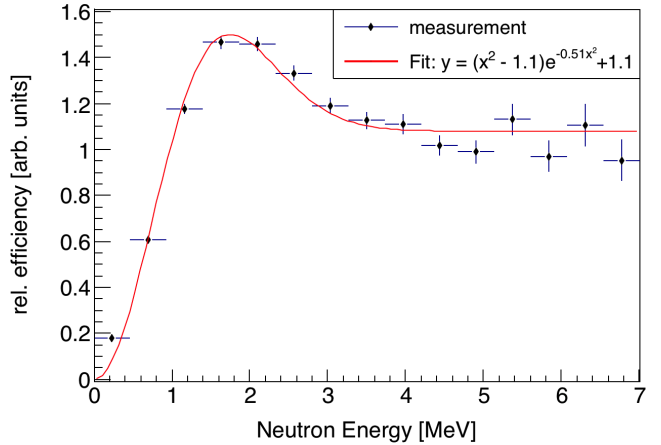


FIG. 4: The overall relative efficiency of the neutron detection system as a function of neutron energy is calculated by dividing the measured energy distribution by the theoretical energy distribution of neutrons from the SF of ^{252}Cf . The fit function is empirical.

issue of cross-talk, see section V B.

The front face of each detector was subject to the highest photon flux due to the scattering of the bremsstrahlung beam from the target. The detection of a photon renders the given detector unable to detect any subsequent fission neutrons from the same pulse due to the detector recovery time. Lead mitigates this problem by reducing photon flux, but has the side effect of scattering neutrons. If a neutron scatters prior to being detected, the ToF measurement and position reconstruction are incorrect. The extent of measurement errors caused by lead shielding were quantified using an MCNP simulation, and, accordingly, 2.5 cm of lead was placed along the front face of the detectors. This diminished photon detection rates to reasonable levels, and, according to the simulation, leads to a root-mean-square error in opening angle and ToF of 1° and 0.3 ns, respectively, due to neutron elastic scattering.

Because of the particularly high photon flux at the sides of all detectors located directly adjacent to the beam, an additional 2" of lead was placed along the sides of these detectors. For the same reason, an additional 2" of lead was also placed along the front faces of the detectors farthest downstream, located at $\pm 30^\circ$ from the beam line. The differences in shielding design among the detectors can be seen in Fig 2.

C. Bremsstrahlung Photon Beam

In order to ensure that all correlated neutrons produced are due to fission, the bremsstrahlung end-point was set to 10.5 MeV, safely below the $(\gamma, 2n)$ threshold of 11.28 MeV for ^{238}U . Aluminum was chosen for the bremsstrahlung radiator because it has a neutron knock-out threshold above the energy of the electron beam,

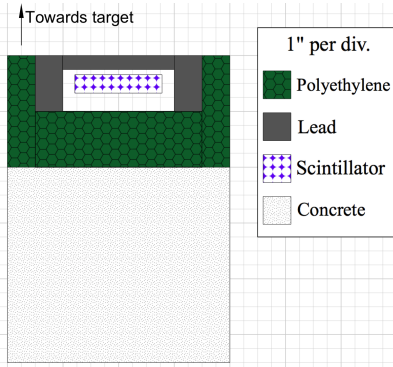


FIG. 5: Detector shielding was designed to reduce the detection of photons, room return, and detector cross-talk.

which ensured that the radiator would not be a source of fast neutrons with the potential to interfere with the experiment. Downstream from the bremsstrahlung radiator is a sweeping magnet that removes charged particles from the photon beam. Next, the beam traveled through a series of polyethylene and lead collimators on its way into the experimental cell in which the target was located (see Fig. 2). Figure 6 shows the energy distribution of photons that reach the target according to an MCNP simulation that modeled the collimation and production of the bremsstrahlung photons.

The electron beam pulse width was set to 3 ns at a repetition rate of 240 Hz with a 1.1 A peak current. The 3 ns pulse width was small compared to the median neutron ToF of 80 ns, and thus made a small contribution to the uncertainty in the neutron energy determination.

303

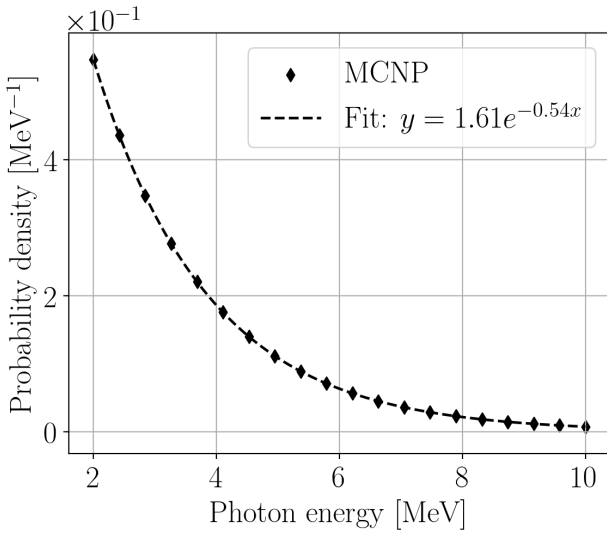


FIG. 6: MCNP simulation of the energy distribution of the bremsstrahlung photons that reach the fission target. Photons with an energy below 2 MeV are excluded.

304

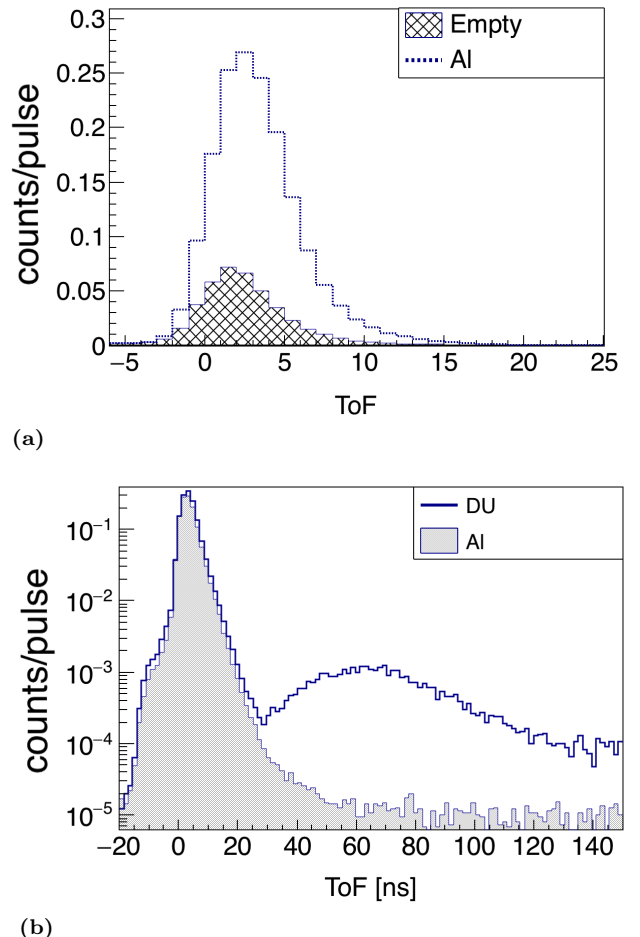


FIG. 7: (a) Comparison between the ToF spectrum of a non-neutron producing target made from Al, to the ToF spectrum produced when no target is used. The large increase in events around 4 ns is due to photons that scatter from the Al target. When no target is in place, sources of the peak include the collimator leading into the experimental cell and the beam dump. The photon peak seen here is used to find the timing offsets that make it so $t = 0$ corresponds to the moment of fission. (b) Comparison between the Al and DU targets show a pronounced increase in events between 35 and 130 ns due to the introduction of neutrons.

D. DU Target

306 A depleted uranium (DU) target in the shape of a thin strip with dimensions of $4 \times 2 \times 0.05$ cm³ was used as the primary target. ²³⁸U was chosen as the fission target because it is an even-even nucleus, and as a consequence, the fission fragments are emitted with a high degree of anisotropy with respect to the photon beam direction [1].

307 Any target comprised of heavy nuclei has a significant potential to scatter fission neutrons before they exit the target, which is a cause for concern, because neutrons that scatter from heavy nuclei are likely to be deflected at large angles, resulting in the measurement of θ_{nn} 's unconnected to the underlying fission kinematics. The rate

305

319 of θ_{nn} 's perturbed by neutron scattering within the ^{238}U
 320 target was estimated by an MCNP simulation to be 6%.
 321 Moreover, it is more likely that neutrons emitted along
 322 the wide, 2 cm, axis of the ^{238}U target undergo a scat-
 323 tering event than neutrons emitted along the thinnest,
 324 0.05 cm, axis. As a result, detectors located collinear to
 325 the widest axis of the target would see relatively fewer
 326 neutrons due to increased scattering along this axis. This
 327 bias is removed by slowly rotating the target about the
 328 vertical axis during data acquisition at a rate of one rota-
 329 tion per 8 seconds. See section V C for discussion of issues
 330 regarding neutron scattering within the fission target.

331

E. Electronics

332 A data acquisition system based on the NIM/VME
 333 standard was used. A schematic of the data acquisition
 334 logic is shown in Figure 8. The PMTs are supplied neg-
 335 ative voltages ranging from 1300 to 1500 V by a LeCroy
 336 1458 high voltage mainframe. Analog signals from the
 337 PMTs were fed into a leading edge discriminator (CAEN
 338 Mod. N841) with input thresholds ranging from 30 mV
 339 to 50 mV. The threshold and supply voltages were deter-
 340 mined individually for each detector to minimize noise,
 341 while simultaneously matching the efficiencies of all the
 342 detectors as closely as possible. Logic signals from the
 343 discriminator were converted to ECL logic and fed into a
 344 CAEN model V1290A TDC. The timing of signals from
 345 the PMTs were always measured relative to a signal from
 346 the accelerator provided at the beginning of each pulse.
 347 Even though a multi-hit TDC was being used, only the
 348 first signal from any given PMT is used each pulse due to
 349 concerns over dead-time within the electronics and signal
 350 reflections within the cables. On the software side, the
 351 CODA 2.5 [14] software package developed by Jefferson
 352 Laboratory was used to read out the data from the TDC
 353 and digitally store it for analysis.

354

III. MEASUREMENT TECHNIQUES

355
356

A. Particle Time of Flight and Energy Determination

357 The ToF of detected particles is used to distinguish
 358 between neutrons and photons and to determine neutron
 359 energy. A particle's reconstructed position is used to de-
 360 termine direction of motion, which is then used to calcu-
 361 late the opening angle between pairs of detected particles.
 362 Position and ToF are each determined using the timing
 363 of coincident signals from both PMTs of a detector.

364 The sum of the times required for scintillation light
 365 to travel from the point of scintillation to both PMTs
 366 is equal to the time required for the light to travel the
 367 full length of the scintillator, which is a constant for light
 368 that travels parallel to the length of the scintillator. This

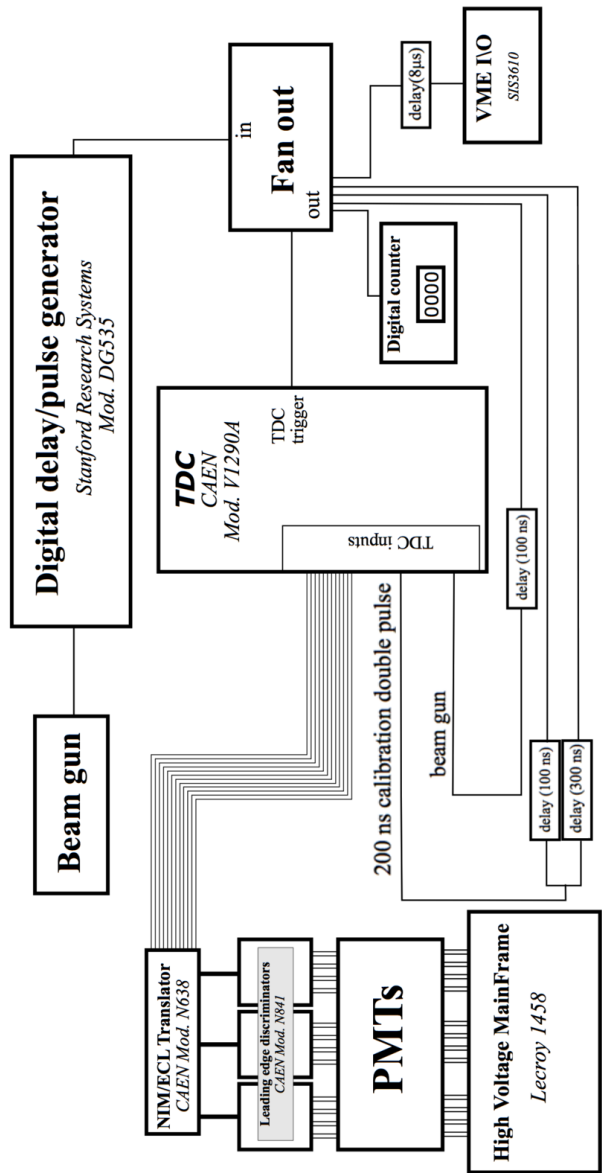


FIG. 8: Wiring diagram of the electronics setup.

369 is supported by data, shown in Fig. 9, which were pro-
 370 duced from a series of tests in which a collimated ^{60}Co
 371 source was placed at seven different locations along a
 372 scintillator. One of the two coincident photons emitted
 373 by ^{60}Co reaches the scintillator and the other is detected
 374 by an auxiliary detector serving as the trigger. The pho-
 375 tons incident on the scintillator have a spot size of less
 376 than 1 cm due to source collimation. These events all
 377 have equal transit time, regardless of the ^{60}Co source's
 378 position.

379 In Figure 9(a), it can be seen that the time required for
 380 the scintillation light to propagate through the scintilla-
 381 tor has a large effect on the timing of each PMT alone,
 382 however, the average of the times of both PMTs is a con-
 383 stant, unaffected by the location at which the particle

undergoes scintillation. For this reason, taking the average of signals from two PMTs is advantageous because it removes the roughly 5 ns timing error that would otherwise exist due to the time required for scintillation light to propagate through the scintillator. The requirement that there be coincident events in both of a detector's PMTs also aids in reducing noise.

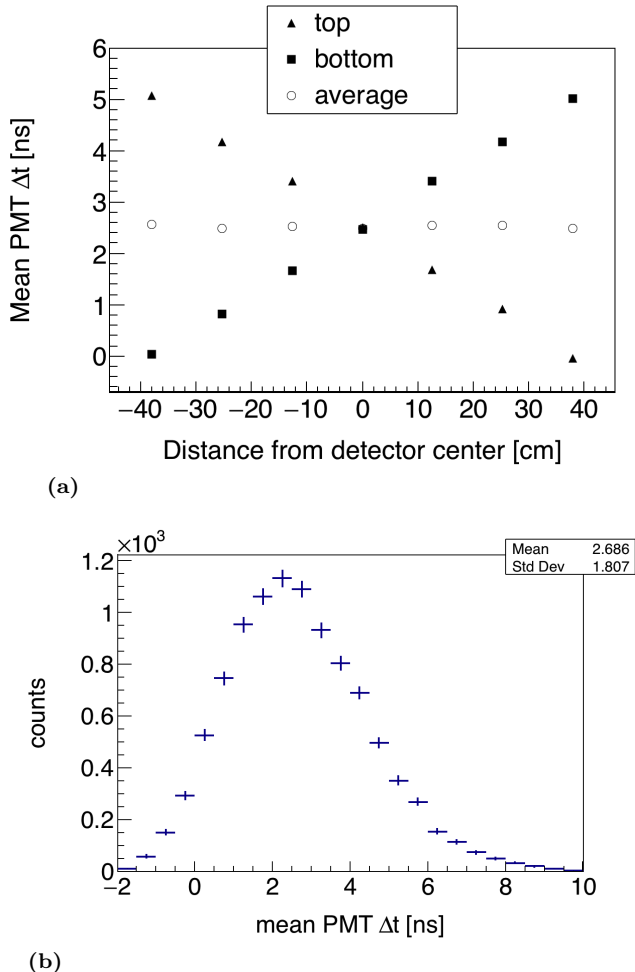


FIG. 9: A collimated ^{60}Co source is used to produce photon events with constant ToF at seven locations along the detector. ^{60}Co produces coincident photons, and one is detected by the scintillator and the other by a separate trigger detector. Δt is the timing of a PMT signal relative to a signal from the trigger detector. In (a), it can be seen that the average between signals from both PMTs does not depend on position. By using the PMT average, there is a reduction in error due to the time required for scintillation light to travel through the scintillator. The uncertainty in ToF measurements is equal to the standard deviation seen in (b), or about ± 2 ns, because all photons from the ^{60}Co source have the same ToF.

391

392

During photofission measurements, ToF is calculated by the following expression:

$$\text{ToF} = t_{\text{avg}}^{\text{PMT}s} - t_{\text{beam}} + C, \quad (1)$$

where $t_{\text{avg}}^{\text{PMT}s}$ is the average of the times of signals from both PMTs of a scintillator, t_{beam} is the time of a signal provided by the accelerator at the beginning of each pulse, and C is a constant timing offset. Any process that produces a timing delay that does not change from pulse to pulse contributes to C . For example, the time required for photons to travel from the bremsstrahlung radiator to the target, the propagation of signals through the cables connecting the PMTs, delays in the electronics, etc.

The value of C , which may be different for each detector, is determined by comparing the timing spectra of the gamma flash produced by a non-neutron producing aluminum target, to that produced when no target is used. The difference between these two spectra reveals a prominent peak in the ToF spectrum due to photons that scatter from the aluminum target. These photons must travel 125 cm to reach the center of any detector and 130 cm to reach the top, for which it takes light 4.2 ns and 4.3 ns to travel, respectively. The value of C used for each detector is equal to the value that places the time corresponding to the peak of the target-induced gamma flash at 4 ns.

Under the assumption that the neutrons are non-relativistic and travel directly from the target to the detectors unimpeded, the calculation of neutron energy from ToF is straightforward. The assumption that neutrons predominantly travel to the detectors unimpeded was validated by MCNP simulations examining the scattering of fission neutrons within the fission target and detector shielding. These simulations are discussed in sections II D and II A.

B. Particle Position Reconstruction

Each detector is not capable of measuring the position of a detected particle along the axes parallel to its width (15.24 cm) or depth (3.81 cm), which contributes $\pm 3^\circ$ to the total angular uncertainty. The position of a detected particle along the 76.2 cm length of the scintillator is calculated using the timing difference of signals from both of a detector's PMTs. Assuming that scintillation light travels from an initial point, let it be x cm from the center of a scintillator, to both PMTs at a velocity that is constant with respect to the scintillator's length-wise axis, then the difference between the times at which the light will reach each PMT ($\Delta t^{\text{PMT}s}$) is given by:

$$\begin{aligned} \Delta t^{\text{PMT}s} &= t^{\text{PMT}_1} - t^{\text{PMT}_2} \\ &= \frac{(L/2 + x)n_{\text{eff}}}{c} - \frac{(L/2 - x)n_{\text{eff}}}{c} \\ &= 2x \frac{n_{\text{eff}}}{c}. \end{aligned} \quad (2)$$

Solving for x gives

$$x = \frac{c}{2n_{\text{eff}}} \Delta t^{\text{PMT}s}, \quad (3)$$

468

C. Measurements with ^{252}Cf

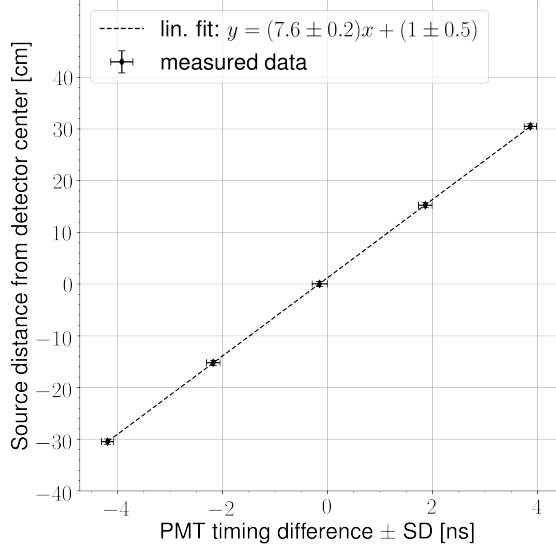


FIG. 10: A collimated ^{60}Co source is used to produce photon events at five different positions along the scintillator. The mean PMT timing difference of events at each position varies linearly with respect to the distance of the ^{60}Co source from the center of the detector. The result of a linear least squares fit to this data is used to calculate the position of detected particles along the length of each scintillator.

440 where t^{PMT_1} and t^{PMT_2} are the times of signals from
 441 each of a detector's PMTs relative to the accelerator gun
 442 pulse, L is the length of the scintillator, c is the speed
 443 of light, n_{eff} is the effective index of refraction of the
 444 scintillation material. A least squares linear fit between
 445 x and Δt^{PMTs} was performed on data gathered using
 446 coincident photons emitted by a collimated ^{60}Co source,
 447 as described in the previous section. The resulting fit
 448 parameters, seen in Fig. 10, are used to find the position
 449 of detected particles.

451 Using the slope of the linear fit in Fig. 10, along with
 452 Eq. 3, an effective index of refraction of the scintillation
 453 material is calculated to be 2.0. This index of refraction
 454 is said to be "effective" because its measurement is sen-
 455 sitive only to the scintillation light's average speed pro-
 456 jected onto the axis parallel to the scintillator's longest
 457 dimension, which is equal to the intrinsic speed of light
 458 in the material only if the light is traveling parallel to the
 459 scintillator's length. While the detection of scintillation
 460 light by both PMTs favors light paths which are par-
 461 allel or nearly-parallel to the scintillator's length, there
 462 is some reflection of detected scintillation light from the
 463 boundaries of the scintillator. This effect contributes to
 464 the ± 9 cm measurement uncertainty in particle position
 465 reconstruction. As a result of these effects, the index of
 466 refraction measured here is $\sim 20\%$ more than the actual
 467 value of 1.58 for PVT.

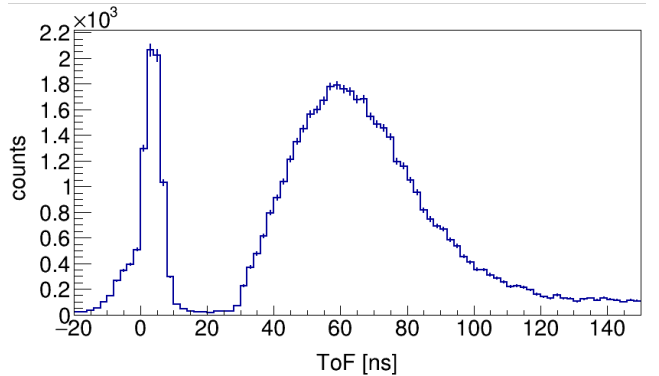


FIG. 11: Measured ToF spectrum from the SF of ^{252}Cf . The sharp peak on the left is due to fission photons, followed by another peak due to fission neutrons.

469 A ^{252}Cf source was placed at the center of the detec-
 470 tion system shown in Fig. 2 in order to measure the n-n
 471 opening angle distribution. Several such past measure-
 472 ments have been performed (see Refs. [8–11]), and serve
 473 as a means to validate the methods used throughout this
 474 study.

475 The ^{252}Cf source produces a cleaner ToF spectrum
 476 than photofission due to the lack of beam related back-
 477 grounds (see Fig. 11), and, therefore, these measurements
 478 have a better signal to noise ratio. Also, there is no con-
 479 cern over the detection of accidental neutron coincidences
 480 because the fission rate of the ^{252}Cf source was about
 481 3,500 fissions/s, making it highly unlikely that multiple
 482 fissions will occur during the electronic acceptance time
 483 window of 150 ns. The beginning of the 150 ns neutron
 484 acceptance time window was triggered by a 2-fold co-
 485 incidence, within a 4 ns window, between two separate
 486 $10 \times 10 \times 5 \text{ cm}^3$ plastic scintillators, one placed above and
 487 the other below the source at a distance of 30 cm. Aside
 488 from this difference in the time window triggering mech-
 489 anism, identical methods were used for both photofission
 490 and SF measurements.

IV. ANALYSIS

492 The efficiency and acceptance of the neutron detection
 493 system varies greatly over its opening angle range of 20°
 494 to 180° , as illustrated in Fig. 12. This is both due to
 495 the neutron detection system's non-spherical symmetry
 496 and to varying efficiency as a function of particle posi-
 497 tion on the detector. In order to give a result that is
 498 sensitive to angular correlations, but is highly insensitive
 499 to detector efficiencies and experimental drifts in PMT
 500 voltage, accelerator current, *etc.*, angular correlation is
 501 determined by dividing a correlated neutron distribution

502 by an uncorrelated neutron distribution. That is,

$$\text{angular correlation} = \frac{nn_{\text{corr}}(\theta)}{nn_{\text{uncorr}}(\theta)}, \quad (4)$$

503 where $nn_{\text{corr}}(\theta)$ is the n-n yield after the subtraction of
 504 accidental n-n coincidences, and $nn_{\text{uncorr}}(\theta)$ is a con-
 505 trived distribution of uncorrelated n-n pairs, which is
 506 produced by pairing neutron events that occurred dur-
 507 ing different pulses. The subtraction of accidental n-n
 508 coincidences to produce $nn_{\text{corr}}(\theta)$ amounts to a 10% cor-
 509 rection, the procedure of which is covered in section IV B.
 510 The construction of $nn_{\text{uncorr}}(\theta)$ is described in detail in
 511 section IV A.

512 A. Cancelation of Detector Efficiencies, Drifts, and 513 Geometric Phase Space

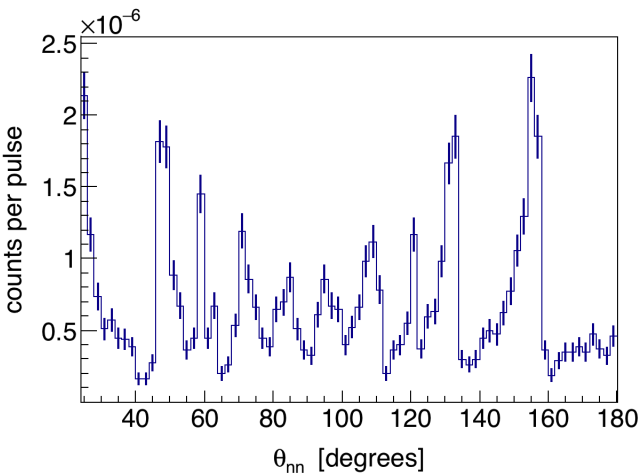


FIG. 12: Raw n-n opening angle yield from the photofission of ^{238}U . This distribution is highly influenced by the detection system's geometry and efficiency.

514 The construction of $nn_{\text{uncorr}}(\theta)$ is achieved by pairing
 515 detected neutrons that were produced during different ac-
 516celerator pulses. The same set of pulses used for $nn_{\text{corr}}(\theta)$
 517 is used here, so each of these pulses individually consist
 518 of the detection of two coincident neutrons. When con-
 519 structing $nn_{\text{uncorr}}(\theta)$, it is desirable that the neutrons
 520 comprising each uncorrelated n-n pair originated from
 521 different pulses that occurred as closely together in time
 522 as possible. A smaller time difference between pulses
 523 that are paired for this purpose increases the chance that
 524 both neutrons were detected under the same experimen-
 525 tal conditions amid any drifting of accelerator current,
 526 PMT voltages, and varying rates of noise. However, some
 527 time difference between the pulses must be allowed so as
 528 not to cause insufficient counting statistics. Accordingly,
 529 uncorrelated n-n pairs used to construct $nn_{\text{uncorr}}(\theta)$ are
 530 formed by neutrons that were detected within 30 minutes
 531 or less of each other.

532 Uncorrelated n-n pairs will have a slightly different
 533 joint energy distribution than correlated n-n pairs, which
 534 could affect the extent to which the effects of detector
 535 efficiency cancel in Eq. 4. This issue is addressed in sec-
 536 tion V A, where it is shown that these differences have
 537 little potential to significantly affect the final result.

538 Figure 13(a) shows the measured yield distribution of
 539 correlated neutrons, $nn_{\text{corr}}(\theta)$, from the photofission of
 540 ^{238}U . The structure seen here is reflective of the under-
 541 lying n-n angular correlations as well as the geometric
 542 acceptance and efficiencies of the neutron detectors. Fig-
 543 ure 13(b) reveals how a clear picture of n-n angular corre-
 544 lations emerges when taking the ratio between $nn_{\text{corr}}(\theta)$
 545 and $nn_{\text{uncorr}}(\theta)$.

547 B. Subtraction of Accidental Coincidences

548 The observation of two uncorrelated signals in the neu-
 549 tron ToF range, whether caused by neutrons, photons,
 550 or noise, is referred to as an *accidental coincidence*. Ac-
 551 cidental coincidences due to noise and photons, which
 552 are estimated using a non-neutron producing aluminum
 553 target (see Fig. 14), amount to about 3% of all coin-
 554 cidences. Accidental coincidences due to neutrons are
 555 minimized by adjusting the accelerator's current so that
 556 there are, on average, less than 1.0 fission per accelerator
 557 pulse, nevertheless, statistical fluctuations in the num-
 558 ber of fissions per pulse result in the production of acci-
 559 dental coincident neutrons that originated from different,
 560 and therefore, uncorrelated fissions. There are also ac-
 561 cidental neutron coincidences caused by the occurrence
 562 of multiple (γ, n) reactions in a single pulse. The energy
 563 integrated (γ, n) cross-section of ^{238}U , weighted by the
 564 bremsstrahlung energy distribution, is about a factor of
 565 5.5 times greater than it is for photofission (see Fig. 15).
 566 As a result, the raw n-n coincident yield will contain a sig-
 567 nificant number of n-n coincidences from multiple (γ, n)
 568 reactions in relation to n-n coincidences from fission. The
 569 presence of accidental n-n coincidences has the effect of
 570 washing out the signal from correlated neutrons.

571 The raw measurement of n-n yield consists of a mix of
 572 correlated and accidental neutron coincidences, that is

$$nn_{\text{raw}}(\theta_{nn}) = nn_{\text{corr}}(\theta_{nn}) + nn_{\text{acc}}(\theta_{nn}), \quad (5)$$

573 where $nn_{\text{raw}}(\theta_{nn})$ and $nn_{\text{acc}}(\theta_{nn})$ are the per-pulse n-n
 574 yields as a function of opening angle, θ_{nn} , for all detected
 575 n-n pairs, and detected accidental n-n pairs, respectively.
 576 As already defined, $nn_{\text{corr}}(\theta_{nn})$ is the per-pulse yield of
 577 detected correlated n-n pairs.

578 Because the n-n coincidences comprising $nn_{\text{acc}}(\theta_{nn})$
 579 consist of two independent detected neutrons, they are
 580 governed by the exact same physics and are subject to
 581 the exact same experimental conditions as n-n coinci-
 582 dences formed by pairing of single neutrons that were
 583 detected during different pulses. Therefore, the open-
 584 ing angle distribution formed by pairing neutrons that

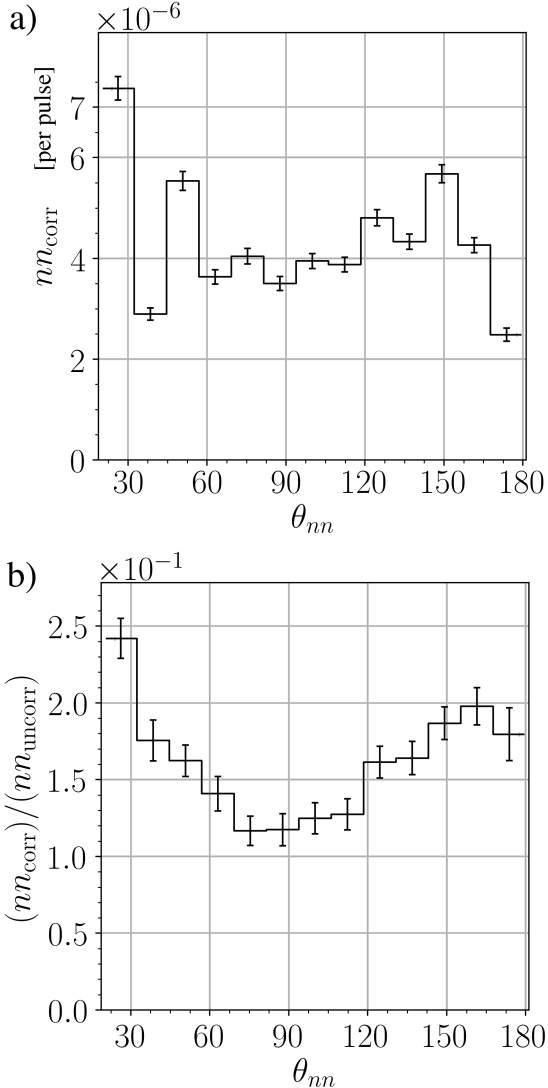


FIG. 13: (a) n-n opening angle distribution from the photofission of ^{238}U before normalization, and, (b) after normalizing to the distribution of uncorrelated n-n events from different pulses. All measured neutrons have an energy greater than 0.4 MeV.

were detected during different pulses, denoted $nn_{dp}(\theta_{nn})$, is proportional to $nn_{acc}(\theta_{nn})$. $nn_{dp}(\theta_{nn})$ is constructed from the set of all possible pulse-pairs formed by pulses that occurred within 0.2 seconds of each other. The restriction in time difference is applied in order to increase the chance that pulse pairs together occurred under similar experimental conditions. There are no other restrictions on which pulses can be used in this case. Thus, many pulse-pairs used for the construction of $nn_{dp}(\theta_{nn})$ will contain no detected neutrons.

While $nn_{dp}(\theta_{nn})$ and $nn_{acc}(\theta_{nn})$ are proportional,

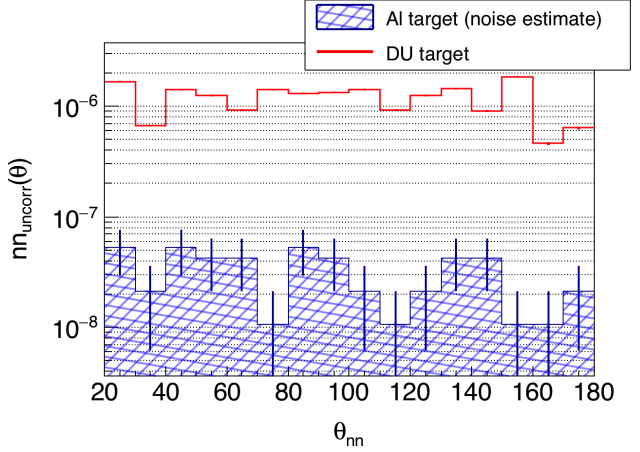


FIG. 14: An Al target was designed to scatter the same number of photons as the ^{238}U target, thus serving as an equivalent non-neutron producing target well-suited for noise estimates. The rate of the detection of coincident events in the neutron ToF range while using the Al target was 3% that of the ^{238}U target. Thus, 3% of coincident events used in the determination of n-n angular correlations in ^{238}U can be attributed to noise.

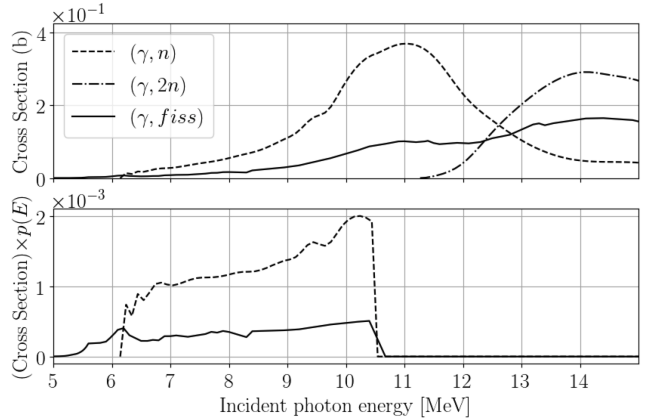


FIG. 15: (top) ENDF cross-sections of $(\gamma, f fiss)$, direct (γ, n) , and direct $(\gamma, 2n)$. (bottom) Cross-sections weighted by the simulated relative rate of bremsstrahlung photons that reach the target as a function of photon energy. The integrated cross-sections of (γ, n) is 5.5 times greater than for $(\gamma, f fiss)$.

⁵⁹⁸ $nn_{acc}(\theta_{nn})$ is not equal to $nn_{dp}(\theta_{nn})$, because there are, ⁵⁹⁹ on average, more detected neutrons per pulse-pair than ⁶⁰⁰ per pulse. As the following analysis shows, $nn_{acc}(\theta_{nn}) =$ ⁶⁰¹ $\frac{1}{2}nn_{dp}(\theta_{nn})$, under the condition that $nn_{acc}(\theta_{nn})$ is nor- ⁶⁰² malized to the number of pulses and $nn_{dp}(\theta_{nn})$ to the ⁶⁰³ number of pulse-pairs looked at. When looking at single ⁶⁰⁴ pulses, the probability of there being a detected uncorre- ⁶⁰⁵ lated n-n pair is denoted by P_{sp}^{n-n} , and when looking at ⁶⁰⁶ pulse-pairs, by P_{dp}^{n-n} . Thus, P_{sp}^{n-n} and P_{dp}^{n-n} determine the ⁶⁰⁷ relative rates of $nn_{acc}(\theta_{nn})$ and $nn_{dp}(\theta_{nn})$, respectively. ⁶⁰⁸ The statistics of the detected uncorrelated neu- ⁶⁰⁹ trons per pulse is assumed to follow a Poisson distribu- ⁶¹⁰ tion, which describes the occurrence of independent ran-

611 dom events. Accordingly, the probability of the detection
612 of k uncorrelated neutrons in a given pulse is

$$p(k) = \frac{e^{-\lambda} \lambda^k}{k!}, \quad (6)$$

613 where λ represents the mean number of uncorrelated de-
614 tected neutrons per pulse. In principle, λ equals the total
615 number of detected uncorrelated neutrons divided by the
616 total number of pulses. Determination of λ cannot be
617 done in practice, because one would need to know which
618 pairs of detected neutrons are correlated. However, the
619 largest possible value for λ is the total number of de-
620 tected neutrons divided by the total number of pulses, as
621 this quantity counts all detected neutrons, whether they
622 are correlated or uncorrelated. For this work, that places
623 an upper bound on λ of 5.5×10^{-3} detected uncorrelated
624 neutrons per pulse, which is small enough to truncate all
625 terms beyond the leading term in the following analysis.

626 Because P_{sp}^{n-n} represents the probability of the detec-
627 tion of two uncorrelated neutrons in a single pulse, P_{sp}^{n-n}
628 is equal to $p(2)$, as per Eq. 6. Thus,

$$\begin{aligned} P_{sp}^{n-n} &= \frac{e^{-\lambda} \lambda^2}{2!} \\ &\approx \frac{\lambda^2}{2} + \mathcal{O}(\lambda^3). \end{aligned} \quad (7)$$

629 When considering the case of P_{dp}^{n-n} , recall that, in
630 this case, uncorrelated n-n pairs are formed by exam-
631 ining pulse-pairs. Here, an uncorrelated n-n pair occurs
632 when there is a detected neutron in both pulses. Because
633 all terms beyond the leading term are being truncated,
634 pulse-pairs in which one or both of the pulses comprise
635 two or more detected neutrons do not need to be con-
636 sidered. Thus, P_{dp}^{n-n} is equal to the probability of there
637 being exactly one detected neutron in each pulse, which
638 is the square of the probability of there being exactly one
639 detected neutron in a single pulse, namely, $p(1)^2$. Thus,
640 again using Eq. 6,

$$\begin{aligned} P_{dp}^{n-n} &= (e^{-\lambda} \lambda)^2 \\ &\approx \lambda^2 + \mathcal{O}(\lambda^3). \end{aligned} \quad (8)$$

641 Because P_{dp}^{n-n} and P_{sp}^{n-n} determine the relative rates of
642 $nn_{dp}(\theta_{nn})$ and $nn_{acc}(\theta_{nn})$, respectively, and because the
643 two distributions have the same shape, from Eq.'s (8)
644 and (7), it follows that

$$nn_{acc}(\theta_{nn}) = \frac{1}{2} nn_{dp}(\theta_{nn}). \quad (9)$$

645 Finally, from Eq.'s 9 and 5, the distribution of solely
646 correlated n-n pairs can be recovered from the raw mea-
647 surement as follows

$$nn_{corr}(\theta_{nn}) = nn_{raw}(\theta_{nn}) - \frac{1}{2} nn_{dp}(\theta_{nn}). \quad (10)$$

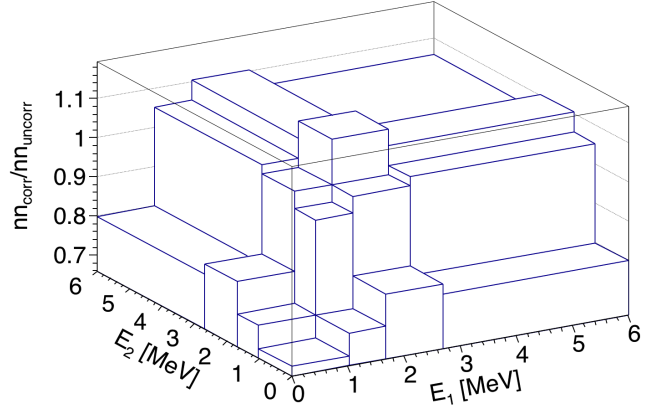


FIG. 16: The z-axis represents the ratio between the correlated and uncorrelated rates of binned n-n energies. The energy bins are chosen such that each contains an equal number of events, or 1/16th of the total events.

V. POTENTIAL SOURCES OF ERROR

A. Correlated versus uncorrelated n-n energy distribution

649 In order to effectively minimize the dependence of the
650 result on detector geometry/efficiency, the numerator
651 and denominator of Eq. 4 must comprise neutron pairs
652 with a similar energy distribution. Note that accidental
653 coincident neutrons from (γ, n) are completely removed
654 from $nn_{corr}(\theta)$, the numerator in Eq. 4, by the subtrac-
655 tion of accidental coincidences, but are not removed from
656 the denominator, $nn_{uncorr}(\theta)$. This is the reason for us-
657 ing only pulse-pairs that have two events in each pulse
658 when determining the uncorrelated neutron distribution.
659 Doing so increases the selection of neutrons from fission
660 as opposed to (γ, n) .

661 When examining differences between the neutron en-
662 ergy distributions in $nn_{corr}(\theta)$ and $nn_{uncorr}(\theta)$, it is im-
663 portant to consider how the energies of both neutrons
664 forming n-n pairs vary together, or, in other words, their
665 joint energy distribution. Figure 16 shows the ratio be-
666 tween the rates for correlated and uncorrelated n-n pairs
667 of various binned energies. The effect that these dis-
668 crepancies in energy distribution have on the final result
669 can be examined by applying a weighting factor to each
670 event in $nn_{uncorr}(\theta)$ such that a recalculation of the re-
671 sult in Fig. 16 produces a flat curve. A comparison of
672 the determined angular correlation with and without the
673 application of these weighting factors to all uncorrelated
674 n-n events is seen in Fig. 17. The resulting differences in
675 angular correlation are negligible.

B. Detector Cross-talk

681 Cross-talk occurs when, after a particle is detected
682 once, the same particle, by any means, causes a detec-

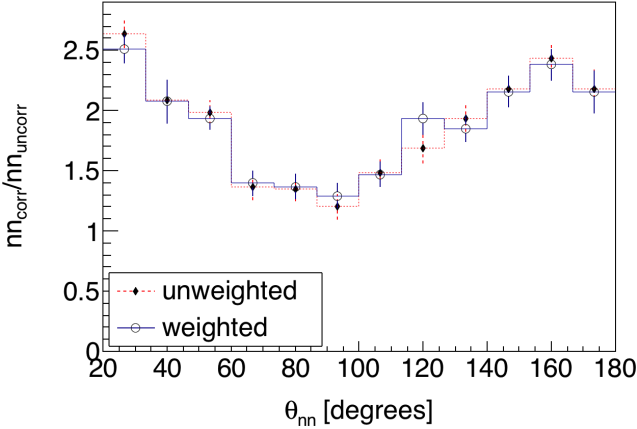


FIG. 17: Each uncorrelated n-n event can be weighted such that the weighted histograms of the joint n-n energy distributions of correlated and uncorrelated n-n pairs are equal. Comparison of the calculated angular correlation results, with and without such weighting factors applied to all uncorrelated n-n events, illustrates that any effects due to the discrepancies in the joint energy distributions of correlated and uncorrelated n-n pairs are negligible.

tion to be registered in a different detector. For example, upon detection, a particle may undergo elastic scattering and then travel into another detector where it is detected again, or, it may produce secondary particles that are detected. The two coincident detections of a cross-talk event are causally correlated, and thus they have the potential to contaminate the signal from correlated fission neutrons. If both detections occur during the ToF range typical for fission neutrons, then the cross-talk event cannot be distinguished from the detection of two correlated neutrons.

Recent works that measured the n-n angular correlations in the spontaneous fission of ^{252}Cf and ^{240}Pu [9, 13] addressed this effect by using an MCNP-PoLiMi simulation to estimate and then subtract cross-talk from their measurements. In this work, the issue of cross-talk is approached differently by employing the use of detector shielding aimed at reducing cross-talk to a negligible rate. By using shielding to reduce cross-talk, this measurement is less dependent on the details of the models used by MCNP-PoLiMi to simulate neutron transport and detection. MCNP-PoLiMi simulations are used in this work only to verify that the effect of cross-talk is negligible.

The scintillators used here are much larger than those used in similar works, such as in Refs. [9, 13], allowing them to be placed much farther from the fission source without causing a detrimental loss in coincidence rates. An increase in the distance between the detectors and the fission source makes this measurement less sensitive to angular uncertainty, which depends directly on the uncertainty in the position of a detected particle due to, for example, the scattering of neutrons from detector shielding. For this reason, larger amounts of shielding can be used without concern of introducing large errors.

Furthermore, the geometry of the neutron detection system makes it kinematically impossible for a neutron to undergo a single scattering event with a proton in one detector, which is the basis for scintillation, and then travel directly into another detector with enough kinetic energy to be detected a second time. For this reason, upon being detected, a neutron must scatter from one or more intermediate nuclei, such as lead or carbon, in order for it to reach another detector with enough energy to be detected again. This fact follows from the conservation of energy and momentum. In order to support the claim that the design of the neutron detection system reduced cross-talk to negligible rates, a detailed MCNP-PoliMi [15] simulation was performed in which a built-in ^{252}Cf source is positioned at the center of a model of the neutron detection system.

1. Simulation of Detector Cross-talk

The cross-talk simulation included all scintillators, shielding, detector supporting structures, and the concrete walls surrounding the experimental cell. MCNP-PoliMi's built-in ^{252}Cf spontaneous fission source was used, which emits neutrons with the correct correlations and multiplicities according to previous measurements. Detector response was modeled using a program included with the MCNP-PoliMi distribution called MP-Post [16]. The model is based on the MeV electron equivalent (MeVee) light output produced by particles as they undergo collisions with carbon and hydrogen within organic plastic scintillators. A minimum deposited energy of 0.4 MeV (equivalent to 0.05 MeVee for neutrons) was assumed for detectable particles, which was chosen because the neutron detection system exhibited a sharp decline in detection efficiency for neutrons below 0.4 MeV.

For neutron collisions with hydrogen, the light output in MeVee, denoted L , is calculated by the following empirically derived formula [16]

$$L = 0.0364\Delta E_n^2 + 0.125\Delta E_n ,$$

where ΔE_n is equal to the loss in the kinetic energy of the neutron due to the collision. Neutron interactions with carbon are assumed to generate a small light output of

$$L = 0.02\Delta E_n .$$

As seen in Fig. 18, this model of the detection process produces a ToF spectrum for the SF of ^{252}Cf that is in good agreement with the measurement.

Figure 19 shows the distribution of cross-talk events and true n-n coincidences as a function of reconstructed opening angle. It is worth noting that, according to this simulation, the effect of cross-talk is not only small, but is also distributed over a wide range of angles rather than being concentrated around 0 degrees as one might expect. Angles greater than 125 degrees are not shown in Fig. 19 because cross-talk events at large angles can

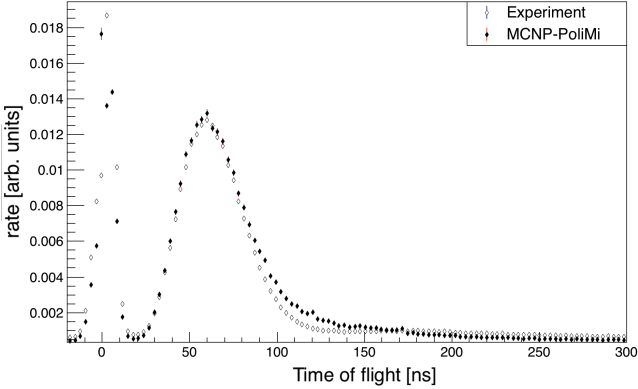


FIG. 18: Measured versus simulated ToF spectrum from the SF of ^{252}Cf . The simulation used the detector response model outlined in ref [16]. The simulated and measured curves are normalized in order to facilitate comparison.

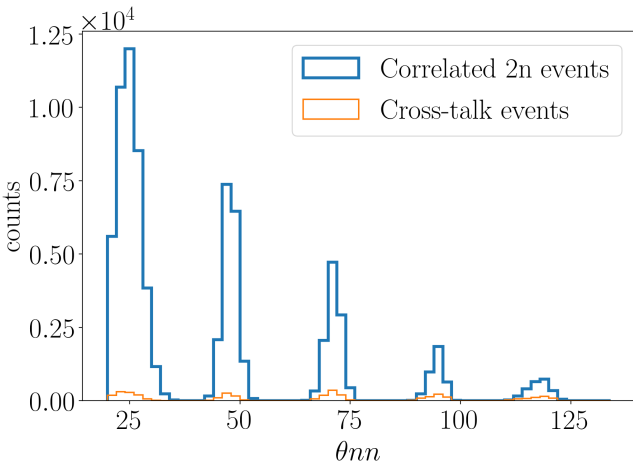


FIG. 19: MCNP-PoLiMi simulation of the number of cross-talk events versus correlated n-n events as a function of reconstructed opening angle. Cross-talk accounted for 3% of total events. Simulated cross-talk events do not occur primarily at small angles, but are instead spread out over a wide range of angles. Any cross-talk occurring at angles larger than 125° will be removed from the experimental data by the cuts applied to neutron ToF.

be readily identified in analysis due to the large amount of time required for a neutron to travel these distances. The simulation was initially performed with 5 cm of lead shielding placed behind the scintillators, and the number of cross-talk events accounted for 11% of the total coincident neutron events. This value fell to 3% when polyethylene was used instead of lead, motivating the placement of 10 cm of polyethylene behind the detectors instead of lead.

778 C. Neutron Scattering within the Target

779 A potential source of error in opening angle measurements is the scattering of emitted neutrons as they tra-

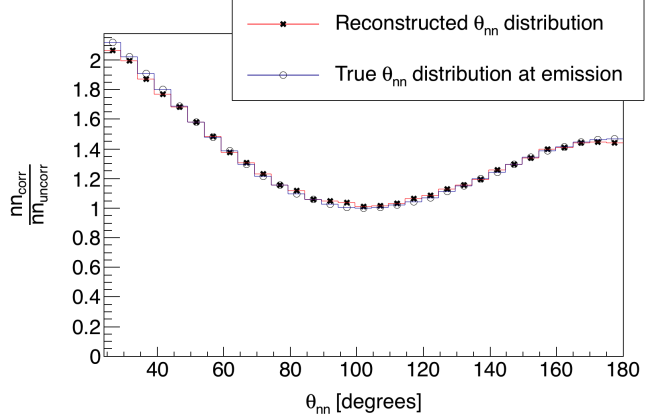


FIG. 20: MCNP-PoLiMi simulation of correlated ^{252}Cf neutrons sampled uniformly throughout a $0.05 \times 2 \times 4 \text{ cm}^3$ U-238 target. The slight difference between the curves is due solely to the elastic scattering of neutrons within the target, since detector physics was not simulated. In the reconstructed θ_{nn} distribution (\star), only neutrons which enter a physical volume at which a detector was located during the experiment are counted. The true θ_{nn} distribution at the moment of emission is also plotted (\circ).

781 verse the fission target. This is a cause for concern be
782 cause when neutrons scatter from heavy nuclides such
783 as ^{238}U , they are likely to be deflected at large angles
784 resulting in n-n opening angles that do not reflect the
785 true underlying fission kinematics. The effect that this
786 has on this work is assessed by MCNP simulations. In
787 summary, for 6% of n-n pairs, at least one neutron out
788 of the two scatters before exiting the target, according to
789 the simulation. This effect does not have a large influ-
790 ence on the measured θ_{nn} distribution according to the
791 simulation data shown in Fig. 20.

792 The rate of elastic scattering is affected by the size
793 and shape of the target. A thin strip is the ideal target
794 shape regarding the rate of neutron elastic scattering per
795 unit of total target volume. See Fig 21 for the simulated
796 elastic scattering rates for both thin strip and cylindrical
797 shaped targets. The simulation indicated that the rate of
798 elastic scattering in cylindrical targets is about a factor
799 of two times greater than in thin strip targets with the
800 same volume.

801 The target's dimensions are small enough that the
802 rate of photon absorption, and thus photo-neutron pro-
803 duction, is virtually uniform throughout the entire tar-
804 get volume. An MCNP-PoLiMi simulation was used
805 to generate ^{252}Cf spontaneous fission events uniformly
806 throughout the target. The SF of ^{252}Cf is used instead
807 of the photofission of ^{238}U because of the current lack
808 of photofission models, however, the underlying fission
809 kinematics are, broadly speaking, the same for the SF of
810 ^{252}Cf and the photofission of ^{238}U . Thus, the two pro-
811 cesses have similar n-n correlations.

812 Section VI B discusses the observation of an unex-
813 pected drop in correlation around 180° in our photofis-

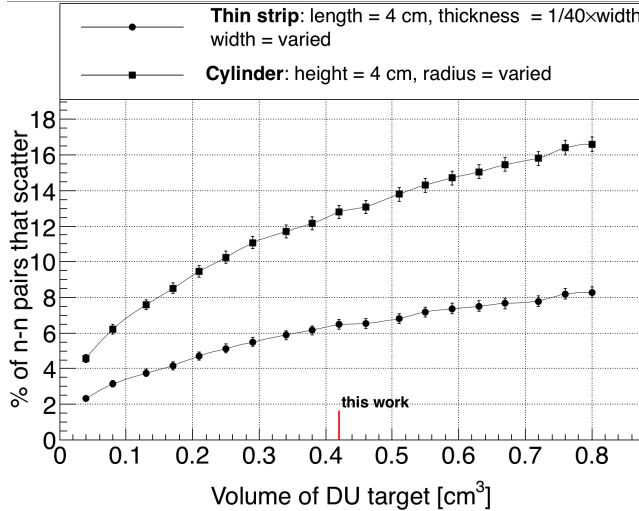


FIG. 21: Result of an MCNP simulation in which n-n pairs, with energies sampled from a typical watt fission spectrum, were generated uniformly throughout the volume of DU targets. The y-axis is the rate of opening angle contamination due to the scattering of, within the DU target in which they were produced, either one or both of a pair of neutrons. The lack of symmetry of a thin strip target can be removed by slowly rotating the target around the vertical axis during data acquisition, making it the optimal target geometry for the minimization of the rate of neutron scattering. The target used in this work had a length of 4 cm, a width of 2 cm, and a thickness of 0.05 cm.

sion of ^{238}U measurement, as seen in Figs. 22 and 23. This motivated a second simulation regarding elastic scattering which examined whether this decrease in the correlation around 180° opening angles reflects the underlying physics of the fission process. In particular, note that throughout these measurements, the target was continuously rotated once per 8 seconds. This means that for the determination of the uncorrelated opening angle distribution, the trajectories of the two neutrons were taken from two different pulses in which the target was at a different orientation for each of them. Additionally, each of the neutrons likely originated from different regions of the target volume. On the other hand, for the same-pulse, correlated neutron measurement, the target was in the same orientation and the two neutrons were generated at the same position in the target. For these reasons, the rates of neutron scattering within the target are not necessarily equal for the same-pulse and different-pulse cases. As such, we investigated whether these differences could cause this apparent decrease in the opening angle distribution near 180° .

Using the correlated ^{252}Cf SF source built-in to MCNP-PoLiMi, the opening angle distribution of neutrons at the moment of emission, labeled *true* in Fig. 20, were compared to that of the neutrons after they have escaped the target, labeled *reconstructed* in Fig. 20. The location of fission events were sampled uniformly throughout the target's volume. The analysis employs the same

technique outlined in section IV A, in which a correlated neutron distribution is divided by an uncorrelated neutron distribution. The correlated neutron distribution is formed by pairing neutrons emitted during the same fission, and the uncorrected distribution by the pairing of neutrons emitted during different fissions. In order to account for the effect of a rotating target on the trajectories of neutrons from different-pulses, the coordinate system was rotated about the vertical axis accordingly for different fission events. The result from this simulation suggests that the rotating $0.05 \times 2 \times 4 \text{ cm}^3$ U-238 target does not, due to neutron scattering, result in a measurable departure from the true n-n opening angle distribution.

VI. RESULTS

The n-n opening angle correlation is calculated using the methods outlined in Sec. IV, in which a correlated neutron yield is divided by an uncorrelated yield. The results are compared with output from FREYA [17] (Fission Reaction Event Yield Algorithm), which was developed by the collaborative efforts of researchers from Lawrence Berkeley National Laboratory, Lawrence Livermore National Laboratory, Los Alamos National Laboratory, and University of Michigan Nuclear Engineering, and has been included in MCNP beginning with version 6.2.

The most recent release of FREYA (version 2.0.3) does not model photofission directly, but instead uses a neutron-induced fission model as an ad hoc photofission model [18]. Modeling photofission in this manner is a crude approximation, unbacked by experimental verification. Nonetheless, due to the current lack of accepted photofission models, the approximate model included in FREYA version 2.0.3 is compared with the results of the present work.

For a given nucleus with Z protons and A total nucleons, the code selects the neutron-induced fission model for a Z(A-1) nucleus, and chooses an incident neutron energy such that the compound ZA nucleus will have, relative to ZA's ground state, an excitation energy that is equal to the energy of the would-be incident photon.

When using FREYA to model photofission in this work, all model parameters, such as level density and partition parameters, were set to their default values for neutron-induced fission. FREYA was configured to use the fission fragment mass distribution, $Y(A)$, and the average total kinetic energy, $\langle \text{TKE} \rangle(A)$, from the ^{238}U photofission measurements described in Ref. [19].

A. n-n angular correlation versus neutron energy

The measured θ_{nn} distribution from the photofission of ^{238}U and the SF of ^{252}Cf are presented with the following

two different types of cuts applied to the energies of neutrons in coincidence: in Figs. 22 (^{238}U) and 24 (^{252}Cf), a minimum energy threshold is applied to both neutrons, and in Figs. 23 (^{238}U) and 25 (^{252}Cf), the energy of both neutrons are required to fall within a specified range

In each of Figs. 22 through 25, the data are reported using two representations: the classic histogram and the kernel density estimate (KDE). When using a histogram to estimate a continuous distribution from the relatively small number of data points obtained in this work, one faces the following dilemma: small bin-widths lead to large uncertainties that are dependent on the chosen bin-width, while large bin-widths obscure potentially useful information. This problem is mitigated by the use of a KDE. A KDE is a method for estimating a continuous probability distribution from a finite set of sampled data points. The kernel was chosen to be the measurement errors in opening angle as determined by a study using coincident photons from a ^{60}Co source, which was placed at different locations along a detector. The measurement errors in θ_{nn} are well-described by a gaussian with a standard deviation of 6° . Mathematical details of the KDE method used in this work are outlined in Ref. [20]. The error bands seen in Figs. 22 through 25 correspond to 68% confidence intervals.

Plotted alongside each measurement is the result of a FREYA simulation. For the measurement of ^{238}U photofission, there were a total of 2,952 n-n coincident events after the subtraction of accidentals, and for the SF of ^{252}Cf , there were 21,882.

925

B. Considering θ_{abs}

While the results reported in the previous section are consistent with the effect of the kinematic focusing of the neutrons due to the recoil of the fission fragments, the data show a small but statistically significant decrease in the n-n opening angle correlation in the region from about 165° to 180° , which can be seen in Figs. 13 and 27, as well as in Figs. 22 and 23. This feature is not evident in previous work on spontaneous and neutron induced fission. The effect is particularly strong for the neutron energy cuts being applied in the upper right plots of both Figs. 22 and 23. A comparison of the observed decrease after 160 degrees with the null hypothesis that the true distribution remains constant after 160 degrees yields a p-value of 0.01. This indicates a 1% probability of obtaining data as compatible with the above hypothesis as the data we observed. A similar effect appears in the results reported in Ref. [12] for the thermal neutron-induced fission of ^{233}U and ^{235}U , but not for the spontaneous fission of ^{252}Cf or the neutron-induced fission of ^{239}Pu .

As previously discussed in section IC, photofission differs from spontaneous and neutron induced fission in that the fission fragments for the photon-induced reaction exhibit an asymmetry in their angle of emission, with the most likely orientation of the fission axis lying perpendic-

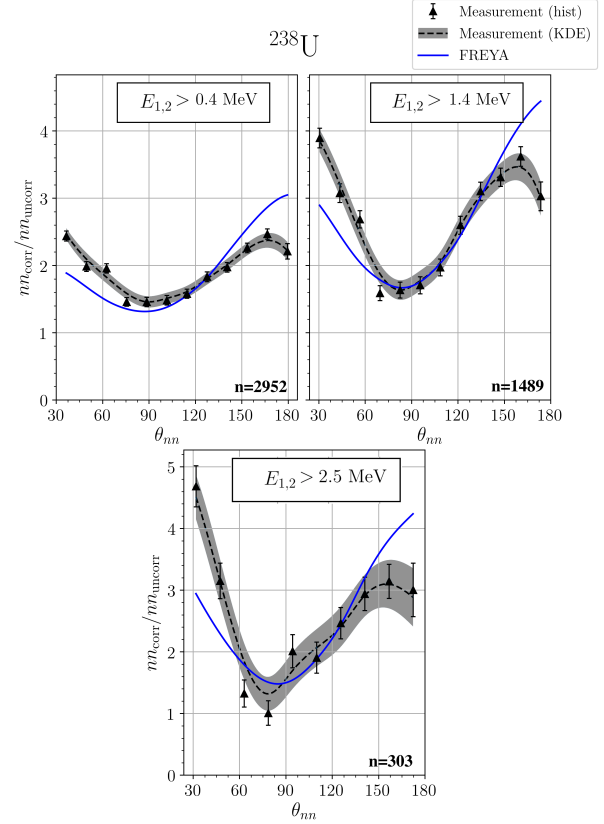


FIG. 22: θ_{nn} distribution with minimum energy threshold cuts applied. The number of events contributing to each plot, n , is shown. Note that the bottom plots of this figure and Fig. 23 are identical.

ular to the direction of the incident photon. With this in mind, the following series of angular cuts were made on the data. Figure 26 shows the distributions of absolute opening angles of the n-n events for three different cuts on the value of the n-n opening angle. For n-n opening angles between 120° and 160° , there is an increased preponderance of both neutrons being emitted around 90° , consistent with the interpretation of kinematic focusing of neutrons coming from fission fragments which are themselves being emitted preferentially at 90° . However, in the opening angle region where the n-n correlation is reduced, from about 160° to 180° , this feature is less prominent.

Furthermore, if one plots the opening angle distributions for the case in which at least one neutron is emitted perpendicular to the incident photon versus the case in which neither neutron is emitted perpendicular to the incident photon (Fig. 27), one sees distinct differences. The fact that there are overall differences is not surprising, because in one case (Fig. 27 solid line) at least one neutron preferentially receives a kinematic boost from a fission fragment and in the other case (Fig. 27 dotted line) neither neutron does. However, the fact that the n-n correlation is reduced at 180° in opening angle when at least one of the neutrons is emitted along the pre-

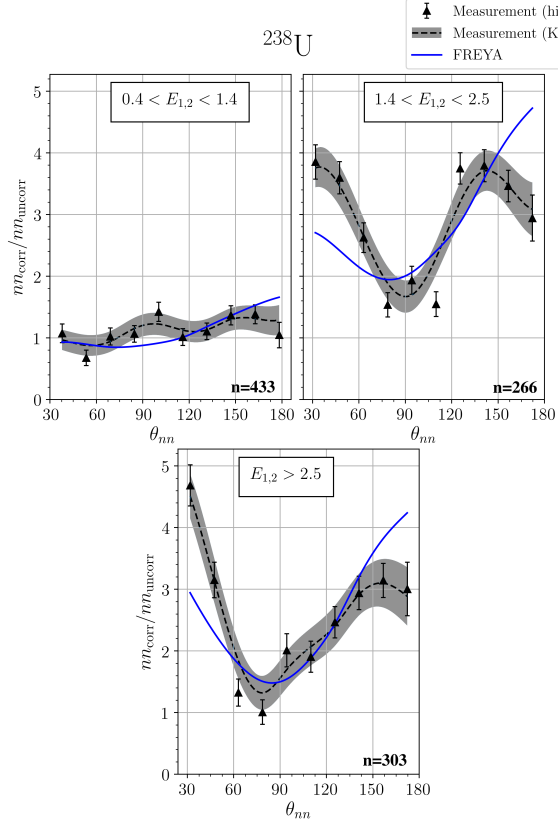


FIG. 23: θ_{nn} distribution with cuts requiring that the energy of both coincident neutrons be within the specified range. The number of events contributing to each plot, n , is shown. Note that the bottom plots of this figure and Fig. 22 are identical.

ferred fission axis is unexpected. This is a feature which does not seem to appear in either neutron-induced fission, previous measurements on spontaneous fission, or our present measurement on spontaneous fission. The photofission of the even-even ^{238}U nucleus seems to be unique in this regard. The attribution of this effect to the geometric coverage of the neutron detection system or to neutron elastic scattering within the target was ruled out using simulations, as discussed in section V C.

These data are consistent with two possible explanations relating to the unique feature of the asymmetric angular emission of fission fragments in photofission. First, the neutrons may indeed be emitted isotropically in the rest frame of the fission fragment, but one fragment essentially shadows the neutrons emitted from the other fragment, either through absorption or scattering. Second, that there is, due to unknown reasons, a decrease in neutron emission along the fission axis. If it is the former case, then this effect has the potential to shed light on the time dependence of neutron emission, since shadowing would likely depend on the fission fragment separation. A definitive interpretation of this decreased n-n correlation for large opening angles in photo-fission

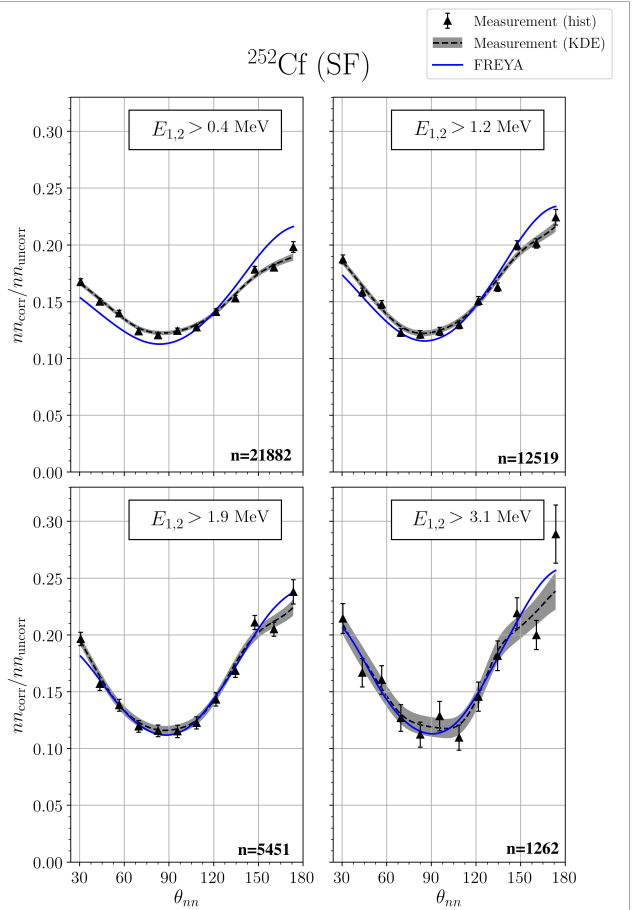


FIG. 24: θ_{nn} distribution a minimum energy threshold cuts applied. The number of events contributing to each plot, n , is shown. Note that the lower right plots of this figure and Fig. 25 are identical.

requires further study.

VII. CONCLUDING REMARKS

Neutron-neutron angular correlations in the photofission of ^{238}U were measured using 10.5 MeV end-point bremsstrahlung photons produced via a low duty factor, pulsed linear electron accelerator. The measured angular correlations reflect the underlying back-to-back nature of the fission fragments. The method of analysis used a single set of experimental data to produce an opening angle distribution of correlated and uncorrelated neutron pairs. A ratio is taken between these two sets to provide a self-contained result of angular correlations, in that the result is independent of neutron detector efficiencies. Neutron-neutron angular correlation measurements were also made using neutrons from the spontaneous fission of ^{252}Cf and show good agreement with previous measurements.

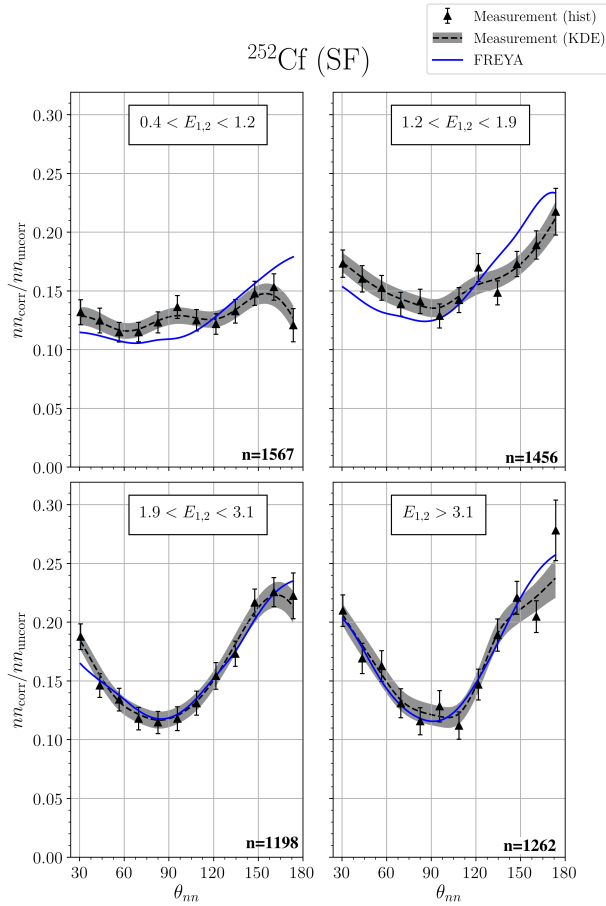


FIG. 25: θ_{nn} distribution with cuts requiring that the energy of both coincident neutrons be within the specified range. The number of events contributing to each plot, n , is shown. Note that the lower right plots of this figure and Fig. 24 are identical.

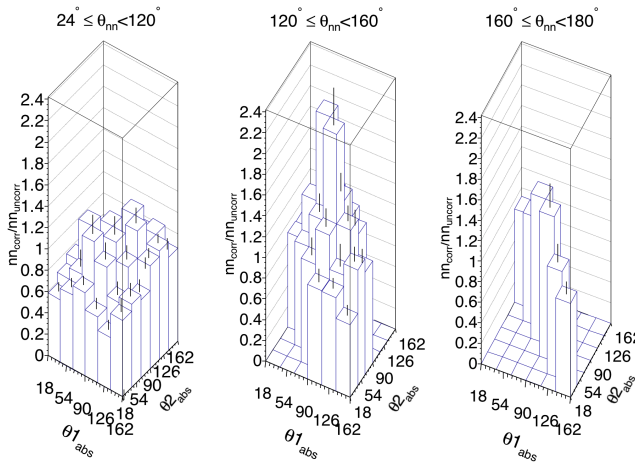


FIG. 26: Correlation is shown between the angles of each neutron with respect to the incident photon beam, denoted by θ_{1abs} and θ_{2abs} . Empty bins exist because of intrinsic geometrical phase-space.

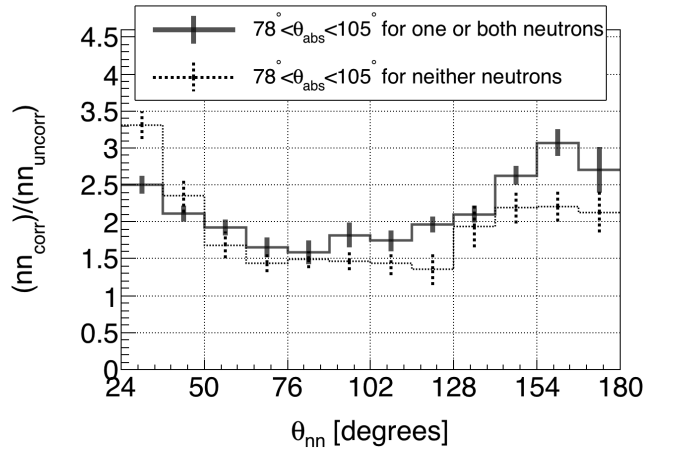


FIG. 27: Requiring that at least one of the coincident neutrons be emitted nearly perpendicular to the photon beam (solid line) produces an opening angle distribution that is different from that produced when it is required that both neutrons are emitted nearly parallel to the photon beam.

Measured n-n opening angle distributions from the photofission of ^{238}U are in great disagreement with the ad hoc photofission model included in FREYA version 2.0.3. This is expected, because the model is only a crude approximation which uses a neutron-induced model to approximate photofission. The present measurement will be useful for fine-tuning photofission models included in future releases of FREYA.

In addition, we report for the first time a pronounced anomaly in the n-n angular distributions from photofission, in which the rate of neutron emission at opening angles near 180° is diminished, resulting in a local maximum at about 160° instead of the expected 180° . We offer two possible explanations for this effect. First, the neutrons may indeed be emitted isotropically in the rest frame of the fission fragment, but one fragment essentially shadows the neutrons emitted from the other fragment, either through absorption or scattering. Second, that there is, due to unknown reasons, a decrease in neutron emission along the fission axis. While these measurements do not provide a definitive interpretation of this decreased n-n correlation for large opening angles in photofission, further study has the potential to shed light on the time evolution of neutron emission in photofission. These first measurements of n-n correlations in photofission have the potential to provide the impetus for future modeling of the fundamental physics of fission.

VIII. ACKNOWLEDGMENTS

This work has been supported by the National Nuclear Security Administration, grant DE-NA002488. We wish to thank the staff of the Idaho Accelerator Center for their assistance in this work. We also wish to acknowl-

¹⁰⁴⁷ edge early contributions to this work by our friend and ¹⁰⁴⁸ colleague the late David V. Jordan of the Pacific North-
¹⁰⁴⁹ west National Laboratory.

- [1] S Nair, D B Gayther, B H Patrick, and E M Bowey. ¹¹⁰⁶
 Fission-neutron and fragment angular distributions from ¹¹⁰⁷
 threshold photofission of ^{232}Th and ^{238}U . *Journal of* ¹¹⁰⁸
Physics G: Nuclear Physics, 3(7):965, 1977. URL <https://stacks.iop.org/0305-4616/3/i=7/a=010>. ¹¹¹⁰
- [2] J. T. Caldwell, E. J. Dowdy, R. A. Alvarez, B. L. ¹¹¹¹
 Berman, and P. Meyer. Experimental determination ¹¹¹²
 of photofission neutron multiplicities for ^{235}U , ^{236}U , ¹¹¹³
 ^{238}U , and ^{232}Th using monoenergetic photons. *Nu-* ¹¹¹⁴
clear Science and Engineering, 73(2):153–163, 1980. doi: ¹¹¹⁵
 10.13182/NSE80-A18695. URL <https://doi.org/10.13182/NSE80-A18695>. ¹¹¹⁶
- [3] G. A. Petrov. Current status of the search for scission ¹¹¹⁸
 neutrons in fission and estimation of their main charac- ¹¹¹⁹
 teristics. *AIP Conference Proceedings*, 798(1):205–212, ¹¹²⁰
 2005. ¹¹²¹
- [4] Harry R. Bowman, Stanley G. Thompson, J. C. D. Mil- ¹¹²²
 ton, and Wladyslaw J. Swiatecki. Velocity and angular ¹¹²³
 distributions of prompt neutrons from spontaneous fis- ¹¹²⁴
 sion of Cf^{252} . *Phys. Rev.*, 126:2120–2136, Jun 1962. doi: ¹¹²⁵
 10.1103/PhysRev.126.2120. URL <https://link.aps.org/doi/10.1103/PhysRev.126.2120>. ¹¹²⁶
- [5] C. Budtz-JÃžrgensen and H.-H. Knitter. Simultane- ¹¹²⁸
 ous investigation of fission fragments and neutrons in ¹¹²⁹
 ^{252}Cf (SF). *Nuclear Physics A*, 490(2):307 – 328, 1988. ¹¹³⁰
 ISSN 0375-9474. doi:[https://doi.org/10.1016/0375-9474\(88\)90508-8](https://doi.org/10.1016/0375-9474(88)90508-8). URL <http://www.sciencedirect.com/science/article/pii/0375947488905088>. ¹¹³³
- [6] P. Talou, R. Vogt, J. Randrup, M. E. Rising, S. A. ¹¹³⁴
 Pozzi, J. Verbeke, M. T. Andrews, S. D. Clarke, P. Jaf- ¹¹³⁵
 kfe, M. Jandel, T. Kawano, M. J. Marcath, K. Meier- ¹¹³⁶
 bachtol, L. Nakae, G. Rusev, A. Sood, I. Stetcu, and ¹¹³⁷
 C. Walker. Correlated prompt fission data in trans- ¹¹³⁸
 port simulations. *The European Physical Journal A*, 54 ¹¹³⁹
 (1):9, Jan 2018. doi:10.1140/epja/i2018-12455-0. URL ¹¹⁴⁰
<https://doi.org/10.1140/epja/i2018-12455-0>. ¹¹⁴¹
- [7] S. Debenedetti, J. E. Francis, W. M. Preston, and T. W. ¹¹⁴²
 Bonner. Angular dependence of coincidences between ¹¹⁴³
 fission neutrons. *Phys. Rev.*, 74:1645–1650, Dec 1948. ¹¹⁴⁴
 doi:10.1103/PhysRev.74.1645. URL <https://link.aps.org/doi/10.1103/PhysRev.74.1645>. ¹¹⁴⁵
- [8] J. S. Pringle and F. D. Brooks. Angular correla- ¹¹⁴⁷
 tion of neutrons from spontaneous fission of ^{252}Cf . ¹¹⁴⁸
Phys. Rev. Lett., 35:1563–1566, Dec 1975. doi: ¹¹⁴⁹
 10.1103/PhysRevLett.35.1563. URL <https://link.aps.org/doi/10.1103/PhysRevLett.35.1563>. ¹¹⁵¹
- [9] J. M. Verbeke, L. F. Nakae, and R. Vogt. Neutron- ¹¹⁵²
 neutron angular correlations in spontaneous fission of ¹¹⁵³
 ^{252}Cf and ^{240}Pu . *Phys. Rev. C*, 97:044601, Apr 2018. ¹¹⁵⁴
 doi:10.1103/PhysRevC.97.044601. URL <https://link.aps.org/doi/10.1103/PhysRevC.97.044601>. ¹¹⁵⁵
- [10] Sara A. Pozzi, Brian Wieger, Andreas Enqvist, Shaun D. ¹¹⁵⁷
 Clarke, Marek Flaska, Matthew Marcath, Edward ¹¹⁵⁸
 Larsen, Robert C. Haight, and Enrico Padovani. Corre- ¹¹⁵⁹
 lated neutron emissions from ^{252}Cf . *Nuclear Science and* ¹¹⁶⁰
Engineering, 178(2):250–260, 2014. doi:10.13182/NSE13- ¹¹⁶¹
 1162
- [11] A. M. Gagarski, I. S. Guseva, V. E. Sokolov, G. V. ¹¹⁶³
 Val'Ski, G. A. Petrov, D. O. Krinitsin, D. V. Nikolaev, ¹¹⁶⁴
 T. A. Zavarukhina, and V. I. Petrova. Neutron-neutron ¹¹⁶⁵
 angular correlations in spontaneous fission of ^{252}Cf . *Bulletin of the Russian Academy of Sciences, Physics*, 72: ¹¹⁶⁶
 773–777, July 2008. doi:10.3103/S1062873808060130.
- [12] V. E. Sokolov and G. A. Petrov. Investigation of the ¹¹⁶⁷
 angular dependences of neutron-neutron coincidences from ¹¹⁶⁸
 ^{252}Cf , ^{235}U , ^{233}U and ^{239}Pu fission in search of scission ¹¹⁶⁹
 neutrons. *Proc. XVIII Internat. Seminar on Interaction* ¹¹⁷⁰
of Neutrons with Nuclei (ISSIN-18), pages 108–118, 2010.
- [13] Matthew J. Marcath, Tony H. Shin, Shaun D. Clarke, ¹¹⁷¹
 Paolo Peerani, and Sara A. Pozzi. Neutron angular dis- ¹¹⁷²
 tribution in plutonium-240 spontaneous fission. *Nuclear* ¹¹⁷³
Instruments and Methods in Physics Research, Section ¹¹⁷⁴
A: Accelerators, Spectrometers, Detectors and Associated ¹¹⁷⁵
Equipment, 830:163–169, 9 2016. ISSN 0168-9002. doi: ¹¹⁷⁶
 10.1016/j.nima.2016.05.064.
- [14] Jefferson Lab. CODA 2.6, 2015. URL <https://coda.jlab.org/drupal>.
- [15] Sara A. Pozzi, Enrico Padovani, and Marzio Marseguerra. ¹¹⁷⁷
 MCNP-PoliMi: a Monte-Carlo code for correlation ¹¹⁷⁸
 measurements. *Nuclear Instruments and Methods in Physics* ¹¹⁷⁹
Research Section A: Accelerators, Spectrometers, Detectors ¹¹⁸⁰
and Associated Equipment, 513(3):550 – 558, 2003. ISSN 0168-9002. doi: ¹¹⁸¹
 https://doi.org/10.1016/j.nima.2003.06.012. URL ¹¹⁸²
<http://www.sciencedirect.com/science/article/pii/S0168900203023027>.
- [16] Eric C. Miller, Shaun D. Clarke, Marek Flaska, Sara ¹¹⁸³
 A. Pozzi, and Enrico Padovani. MCNPX-PoliMi post- ¹¹⁸⁴
 processing algorithm for detector response simulations. *JNMM, Journal of the Institute of Nuclear Materials* ¹¹⁸⁵
Management, 40(2):34–41, 12 2012. ISSN 0893-6188.
- [17] Lawrence Berkeley National LaboratoryLawrence Livermore National LaboratoryLos Alamos National LaboratoryUniversity of Michigan Nuclear Engineering. FREYA 2.0.3, 2016. URL <https://nuclear.llnl.gov/simulation/main.html>.
- [18] S. D. Clarke, B. M. Wieger, A. Enqvist, R. Vogt, ¹¹⁸⁶
 J. Randrup, R. C. Haight, H. Y. Lee, B. A. Perdue, E. Kwan, C. Y. Wu, R. A. Henderson, and ¹¹⁸⁷
 S. A. Pozzi. Measurement of the energy and multi- ¹¹⁸⁸
 plicity distributions of neutrons from the photofission ¹¹⁸⁹
 of ^{235}U . *Phys. Rev. C*, 95:064612, Jun 2017. doi: ¹¹⁹⁰
 10.1103/PhysRevC.95.064612. URL <https://link.aps.org/doi/10.1103/PhysRevC.95.064612>.
- [19] Krishchayan, M. Bhike, A. P. Tonchev, and W. Tornow. ¹¹⁹¹
 Fission product yield measurements using monoenergetic ¹¹⁹²
 photon beams. In *European Physical Journal Web of* ¹¹⁹³
Conferences, volume 146 of *European Physical Journal Web of* ¹¹⁹⁴
Conferences, page 04018, September 2017. doi: ¹¹⁹⁵
 10.1051/epjconf/201714604018.
- [20] Kyle Cranmer. Kernel estimation in high-energy ¹¹⁹⁶
 physics. *Computer Physics Communications*, 136(3): ¹¹⁹⁷
 198–207, 2001.